# Mechanisms in non-heme iron oxidation catalysis

Chen, Juan

# CHAPTER 5

# Heterolytic O-O bond cleavage in a N5 coordinated non-heme iron(II) complex and the role of comproportionation in the direct generation of oxoiron(IV)

The reaction of the non-heme N5 coordinated iron(II) complex $[(N4Py)Fe^{II}(CH_3CN)]^{2+}$ with substoichiometric (0.5 equiv) $H_2O_2$ results in the direct formation of an Fe(IV)=O species through the heterolytic cleavage of O-O bond of an $Fe^{II}$-OOH intermediate. Disproportionation of the Fe(IV)=O with its Fe(II) precursor proceeds rapidly to form the corresponding iron(III) complex. The solvent ($H_2O$, methanol, and acetonitrile) and temperature dependence of the disproportionation is discussed with DFT calculations that corroborate the proposed mechanism.

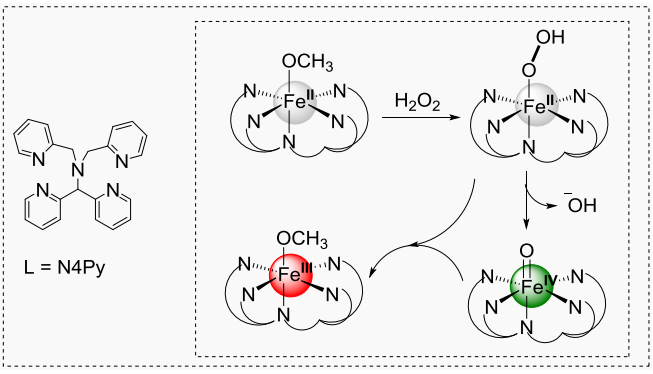


Manuscript to be submitted:

Juan Chen, Apparao Draksharapu, Davide Angelone, Duenpen Unjaroen, Sandeep K. Padamati, Ronald Hage, Carole Duboc, Marcel Swart, Wesley R. Browne

## 5.1 Introduction

High valent Fe(IV)=O species are frequently invoked as the active species in the oxidation of organic substrates by both heme and non-heme enzymes.[1,2] Whereas nature employs oxygen and electron donors (e.g., decarboxylation), the generation of non-heme biomimetic Fe(IV)=O species from Fe(II) complexes, supported by tetradentate N4 (TMC, BPMCN, etc.) and pentadentate N5 (N4Py, MeN4Py, Bn-TPEN etc.) ligands, requires two-electron oxidants, such as PhIO,[3–5] m-CPBA and peracetic acid,[6,7] and hydroperoxides (e.g., $H_2O_2$ and tert-butyl hydroperoxide).[3,8,9]

Under conditions employed commonly in catalytic oxidations with $H_2O_2$ with non-heme iron complexes typically show rapid initial oxidation of the catalyst to the Fe(III) state.[10] Thereafter, during catalysis, one electron oxidation through O-O bond homolysis in Fe(III)OOH species yields the corresponding Fe(IV)=O species and an equivalent of hydroxyl radicals. As a consequence, the reaction between Fe(II) species and $H_2O_2$ has received scant attention, with notable exceptions such as that by Que, Comba, and coworkers,[11,12] whom noted that iron(II) reacts with a slight excess of $H_2O_2$ to form Fe(IV)=O species for several synthetic non-heme iron(II) complexes.

From a catalytic perspective, understanding the relevance of O-O heterolysis to form Fe(IV)=O species is of special importance in oxygen atom transfer reactions since the complex is returned to the Fe(II) state. Hence, there is the possibility of generation of Fe(IV)=O species catalytically without concomitant formation of reactive hydroxyl radicals.

The mechanism for formation, O-O bond heterolysis vs homolysis in the putative $Fe^{II}$-OOH intermediate, remains unclear. For the N5 coordinated $Fe^{II}$(bispidine) complex (**Figure 80**), reaction with $H_2O_2$ in aqueous media yielded an Fe(IV)=O species, attributed to heterolytic cleavage of O-O bond an unobserved $Fe^{II}$-OOH intermediate.[12] However, the low yield (< 60%) of Fe(IV)=O casts doubt on the occurrence of O-O bond heterolysis, in contrast, to the base-catalyzed reaction of the N4 coordinated $[(TMC)Fe^{II}]^{2+}$ complex with stoichiometric $H_2O_2$ (**Figure 80**). The latter forms the corresponding Fe(IV)=O species with over 90% yield. Proton-transfer was proposed to be important in driving the heterolytic O-O bond cleavage step.[11] With the exception of the $[(TMC)Fe^{II}]^{2+}$ complex at -40 $^{o}$C, the direct formation of Fe(IV)=O with sub and near stoichiometric $H_2O_2$ has not been reported. However, similar reactivity in other N4 and N5 systems may in fact be masked by competing reactions, in particular, comproportionation between the Fe(IV)=O species generated and the Fe(II) precursor.

Here, we show that in methanol heterolytic cleavage of the O-O bond of a N5 coordinated Fe(II)-OOH species yields the corresponding Fe(IV)=O species directly. Subsequent comproportionation with the initial Fe(II) complex ultimately yields the Fe(III) complex. A combination of experimental and quantum chemical calculations are used to establish mechanistic insight in the process overall.

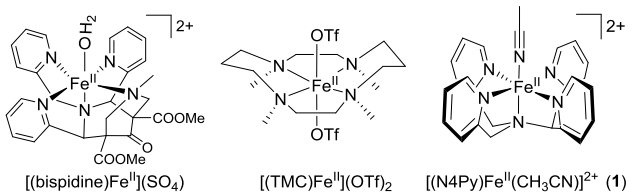


**Figure 80.** Structures of iron complexes discussed in the text.

## 5.2 Results and Discussion

Although, complex **1** reacts only slowly with $H_2O_2$ in acetonitrile, it reacts rapidly in methanol (vide infra) due to prior exchange of the acetonitrile ligand in **1** for methoxide upon dissolution. This aspect is key to understanding the reactivity of the Fe(II)-OOH species as the exchange of methoxide with $H_2O_2$ is rapid (vide infra) and allows for the heterolysis to form Fe(IV)=O and outcompete subsequent comproportionation.

Exchange of $CH_3CN$ in **1** for $-OCH_3$ to form $[(N4Py)Fe(II)(OCH_3)]^+$ (**1-OCH$_3$**) is manifested in a bathochromic shift and broadening and weakening of the visible absorption bands. Addition of acetonitrile (2 vol%) results a 90% recovery of the spectrum of **1** (**Figure 81**), consistent with the difference in redox potentials of **1** and **1-OCH$_3$**, and the higher binding constant of $CH_3CN$ as observed in $H_2O$ also.[13] Addition of 1 vol% $H_2O$ in **1** in methanol results in a further decrease in molar absorptivity and broadening is observed upon addition of water (1 vol%) consistent with exchange of $-OCH_3$ with $H_2O$ (**Figure 81**). In summary, the preference of the sixth ligand for the Fe(II) state follows the order of $CH_3CN$ >> $H_2O$ > $^-OCH_3$.[13] The displacement of aquo and methoxide by hydrogen peroxide is therefore expected to be facile in contrast when acetonitrile is present, based on differences in redox potential.[14] Hence, the rate determining step in the reaction of $H_2O_2$ with **1** in acetonitrile is ligand exchange (**Figure 82**), which is in contrast with that observed in the reaction of $[(TMC)Fe^{II}]^{2+}$ with $H_2O_2$, in which oxidation was observed even at -40 $^oC$.[11]

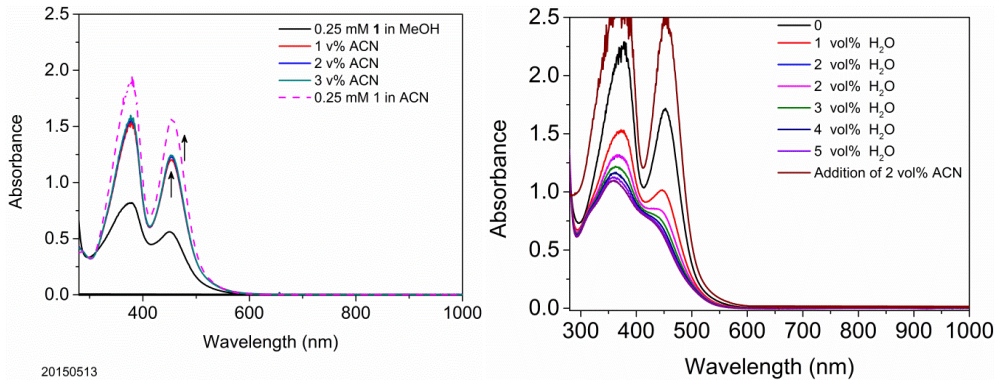


**Figure 81.** UV-vis absorption spectra (left) of **1** (0.25 mM) in methanol (black) after addition of 1 - 3 vol% acetonitrile, and in acetonitrile (magenta). UV-vis absorption spectra (right) of **1** (0.5 mM) in methanol with addition of 1 -5 vol% $H_2O$, followed by addition of 2 vol% acetonitrile.

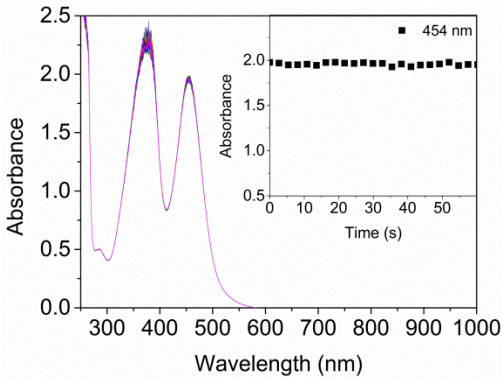


**Figure 82.** UV-vis absorption spectrum changes of **1** (0.25 mM) in acetonitrile after addition of 0.5 equiv $H_2O_2$.

### 5.2.1 Reaction of 1 with near sub-stoichiometric $H_2O_2$

Addition of excess $H_2O_2$ to **1** in methanol leads rapidly to formation of $[(L)Fe(III)(X)]^{2+}$ (X = $^{-}OH/^{-}OCH_3$).[10] Stepwise addition of $H_2O_2$ (50% v/v in $H_2O$, 0.1 equiv per step) to **1** in methanol (**Figure 83**) results in a concomitant stepwise decrease (20% per step) in absorbance (350-500 nm). The decrease is accompanied by the step-wise appearance of a weak absorption band at 692 nm that is characteristic of $[(N4Py)Fe(IV)=O]^{2+}$ (**2**). The absorbance at 692 is nm is greater in $CD_3OD$ with a maximum 12% yield, (**Figure 84** and **Figure 85**). Overall oxidation of **1** to $[(N4Py)Fe(III)(OCH_3)]^{2+}$ was confirmed by the characteristic X-band EPR spectrum with S = ½ signal (g = 2.29, 2.12, and 1.96, **Figure 86**), as well as resonance Raman (vide infra) with ca. 0.5 equiv $H_2O_2$, consistent with a 2:1 stoichiometry between **1** and $H_2O_2$.

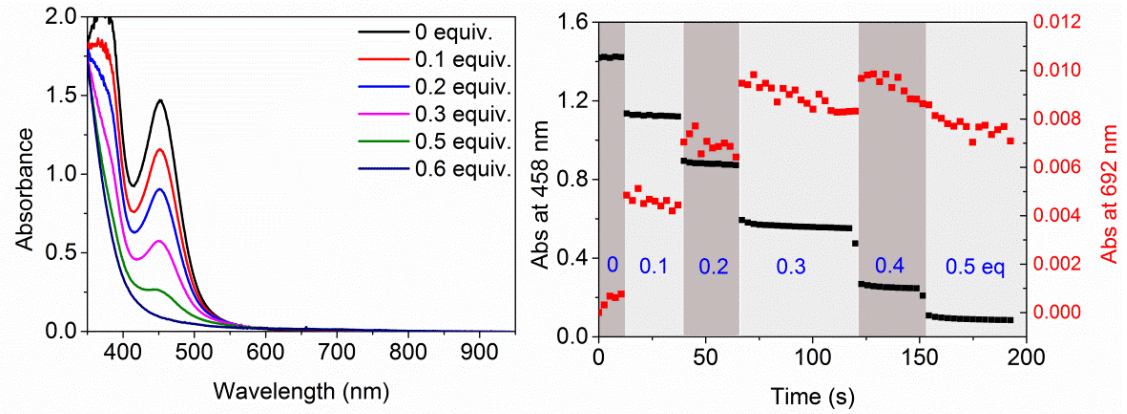


**Figure 83.** (left) Stepwise addition of $H_2O_2$ to **1** (0.5 mM) in $CH_3OH$ at 21 °C. UV-vis absorption spectra; initial (black) and at 0.1 eq (red), 0.2 eq (blue), 0.3 eq (magenta), 0.4 eq (green) and 0.5 eq (navy) of $H_2O_2$. Inset: expansion of 560 – 950 nm region. (right) Corresponding change in absorbance at 454 nm (black) and 696 nm (red)

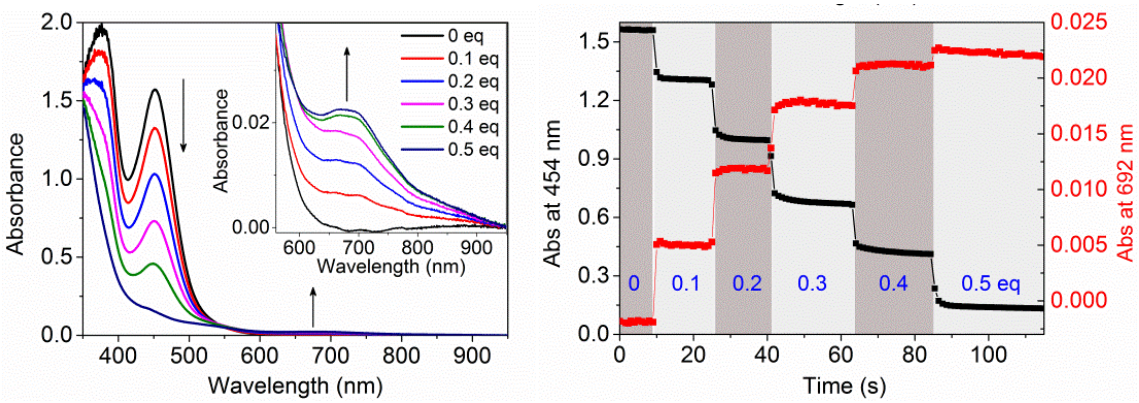


**Figure 84.** (left) Stepwise addition of $H_2O_2$ to **1** (0.5 mM) in $CD_3OD$ at 21 °C. UV-vis absorption spectra; initial (black) and at 0.1 equiv (red), 0.2 equiv (blue), 0.3 equiv (magenta), 0.4 equiv (green) and 0.5 equiv (navy) of $H_2O_2$. Inset: expansion of 560 – 950 nm region. (right) Corresponding change in absorbance at 454 nm (black) and 692 nm (red).

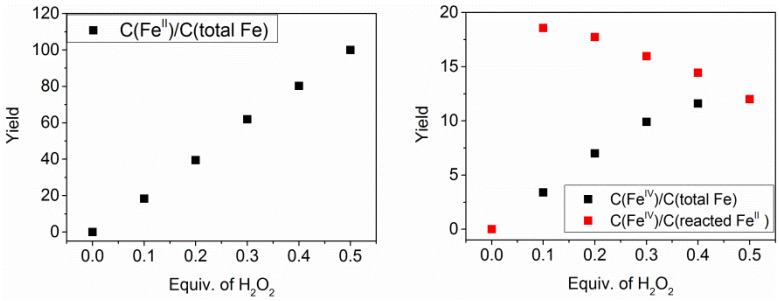


**Figure 85.** (left) Ratio of reacted **1** to the total iron with step-wise addition of $H_2O_2$; (right) Ratio of formed **2** to the total iron (black) and to the reacted **1** (Red) with step-wise addition of $H_2O_2$.

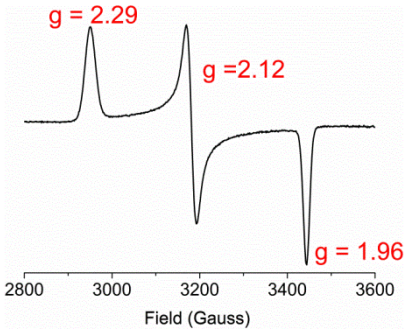


**Figure 86.** X-band EPR spectra of the flash frozen (at 77 K) solution of **1** in methanol after addition of 0.5 equiv $H_2O_2$.

Raman spectroscopy ($\lambda_{exc}$ = 355 nm, **Figure 87**) shows a band at 554 $cm^{-1}$ appearing and increasing with the addition of $H_2O_2$ from 0.1 equiv to 0.6 equiv The band is assigned to $\nu_{str}$ = Fe-O on the basis of the shift from 554 $cm^{-1}$ to 531 $cm^{-1}$ ($\Delta\nu$ = 23 $cm^{-1}$) in $CD_3OD$ but absence of a shift in $CH_3OD$. The shift is also consistent with the DFT predicted shift (21 $cm^{-1}$) for $[N4PyFe(III)(OCH_3)]^{2+}$ to $[N4PyFe(III)(OCD_3)]^{2+}$. The resonance enhancement of this band at 355 nm is consistent with the assignment of the absorption band as a ligand to metal charge transfer transition of $[(N4Py)Fe(III)(OCH_3)]^{2+}$, which is close to that of the Fe(III)-$OCH_3$ complex of Bleomycin (530 $cm^{-1}$).[15]

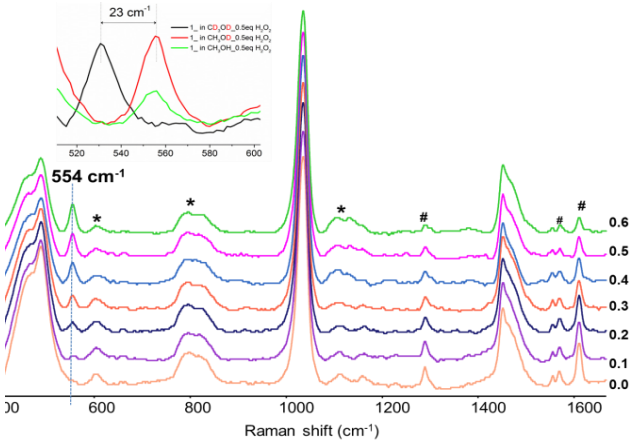


**Figure 87.** Change to the Raman spectrum ($\lambda_{exc}$ 355 nm) of **1** in methanol before and after adding 0.1 to 0.6 equiv $H_2O_2$. The band at 1555 $cm^{-1}$ was assigned to the symmetric stretch mode for $O_2$.[16] * Raman scattering from quartz cuvette. # scattering from **1**. Insert: expansion of 510-570 $cm^{-1}$ region to show 554 $cm^{-1}$ band in $CH_3OH$, $CH_3OD$ and $CD_3OD$.

The 2:1 stoichiometry (**1**/$H_2O_2$) for the conversion of **1** to Fe(III)($OCH_3$) is in contrast with the previously reported near 1:1 ratio in (TMC)FeII/$H_2O_2$ and Fe(II)(bispidine)/$H_2O_2$ reaction system, and the yield of iron(IV)=O is even lower.[11,17] The formation of minor amounts of **2** (Fe(IV)=O), especially in $CD_3OD$, can be either due to homolysis of the O-O bond of an Fe(III)-OOH intermediate (eq 1) as proposed in for the Fe(II)(bispidine) system in methanol[17] or due to heterolysis of the O-O band of an initially formed Fe(II)-OOH species (eq 2).

$$[(L)Fe^{III}\text{-}OOH]^{2+} \longrightarrow [(L)Fe^{IV}{=}O]^{2+} + HO^{\bullet} \quad \text{(eq 1)}$$

$$[(L)Fe^{II}\text{-}OOH]^{+} \longrightarrow [(L)Fe^{IV}{=}O]^{2+} + HO^{-} \quad \text{(eq 2)}$$

The homolytic pathway is unlikely, since addition of excess $H_2O_2$ (50 equiv) to (Fe(III)($OCH_3$)) (**Figure 88**), shows a maximum of Fe(III)OOH ($\lambda_{max}$ = 550 nm). Its subsequent decay is slow ($3.0 \times 10^{-4}$ $s^{-1}$), and contrasts with the spontaneous formation of **2** (Fe(IV)=O) after addition of $H_2O_2$ to **1** (**Figure 84**). These data are consistent with the DFT-calculated $\Delta H^{\ddagger}$ of the O–O bond homolysis of the $[(N4Py)Fe(III)OOH]^{2+}$ complex of 19.6 kcal/mol.[18] Furthermore, complete oxidation of **1** via homolytic cleavage cannot account for the 2:1 stoichiometry, as it would need > 0.5 equiv $H_2O_2$ (1 equiv for oxidation. **1** equiv for homolytic cleavage of O-O bond of Fe(II)-OOH).

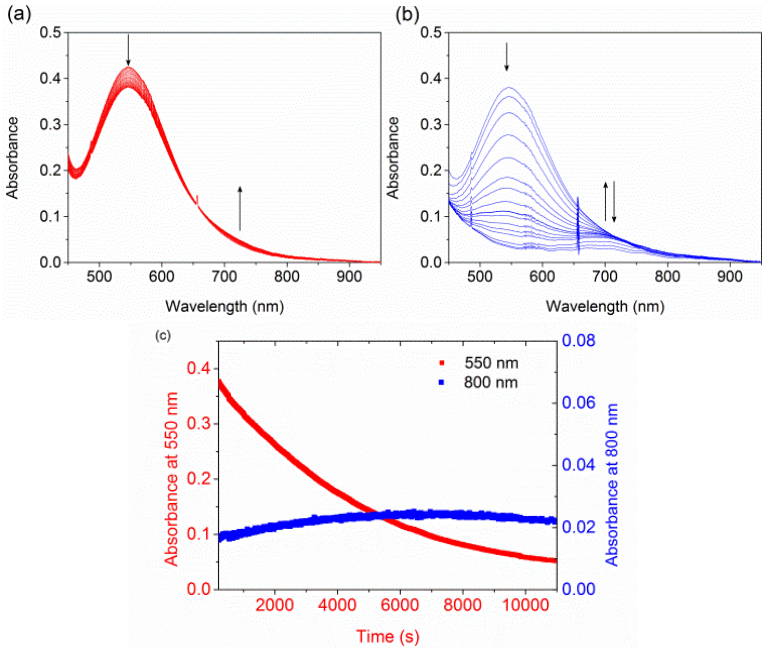


**Figure 88.** UV-vis absorption spectrum changes of $[(N4Py)Fe(III)(OCH_3)]^{2+}$ (**5a**) (0.5 mM) in $CD_3OD$ with addition of 50 equiv $H_2O_2$ at 21 °C, (a) 50 - 200 s, (b) 200 -11000 s, (c) changes of absorbance at 550 nm and 692 nm, respectively.

In contrast, the heterolytic O-O bond cleavage in Fe(II)-OOH (eq 2) is highly exergonic (*vide infra*), as is comproportionation between non-heme Fe(IV)=O species and Fe(II) complexes has been shown to be exergonic in $H_2O$,[19] consistent with the overall 2:1 stoichiometry. The kinetic feasibility of comproportionation under the present conditions was studied further. **2** engages in oxidation of both alcohol (solvent oxidation) as well as $H_2O_2$[20,21], which complicates kinetic analysis of comproportionation in methanol.

Comproportionation of **1** with **2** (Fe(IV)=O), prepared independently (**Figure 89**), in methanol proceeds more rapidly ($6.0 \times 10^{-3}$ $s^{-1}$, **Table 7**) than the oxidation of methanol to formaldehyde by

**2** (**Figure 90**, ($1.8 \times 10^{-3}$ $s^{-1}$, **Table 7**).[22] Furthermore the visible absorbance of **1** decreases concomitantly with the NIR absorbance of **2.** Over the same period, **1** is stable in methanol in the absence of **2.** The final product $[(N4Py)Fe(III)(OCH_3)]^{2+}$ was confirmed by both X-band EPR spectroscopy (**Figure 89**) and resonance Raman spectroscopy (**Figure 90**). As expected, formaldehyde was not formed, confirming that **2** (Fe(IV)=O) does not react significantly with solvent on the same timescale. Indeed the comproportionation of Fe(II) and **2** (Fe(IV)=O) is faster in both $CH_3OH$ and $CD_3OD$ than the reaction of **2** (Fe(IV)=O) with methanol (4 fold) and $CD_3OD$ (20 fold). In $CD_3OD$, the comproportionation is ca. 4 times slower ($1.3 \times 10^{-3}$ $s^{-1}$, **Table 7**, **Figure 91**) than in $CH_3OH$, and increases with an increase in the concentration of $H_2O$ (**Figure 92**), indicative of an inner sphere mechanism for electron transfer between **2** and the Fe(II)-$OH_2$ complex rather than between **2** and **1-OCH$_3$**. This conclusion is supported by the lack of comproportionation -30 $^{o}C$, with the absorption bands for both **1** and **2** remaining unchanged until the addition of 10 vol% of $H_2O$ ($3.9 \times 10^{-3}$ $s^{-1}$, **Table 7**), and accelerating further with 50 vol% of $H_2O$ added ($4.3 \times 10^{-2}$ $s^{-1}$, **Table 7**, **Figure 93**). The comproportionation of **1** with **2** (Fe(IV)=O) in $H_2O$ was reported earlier,[19] in present study the effect of deuteration was studied, (**Figure 94**, 1.12 $s^{-1}$ in $H_2O$ and 0.4 $s^{-1}$ in $D_2O$, **Table 7**) which shows a similar KIE value with that observed in methanol. Hence, the conversion of **1** to (Fe(III)($OCH_3$)) is likely to proceed by ligand exchange from **1-OCH$_3$** to **3** (Fe(II)OOH), followed by heterolytic cleavage of the O-O bond to form $[(N4Py)Fe(IV)=O]^{2+}$ (**2**) and $OH^-$. The formed Fe(IV)=O comproportionates with $[(N4Py)Fe(II)(OCH_3)]^{+}$ (**1-OCH$_3$**) or more likely with $[(N4Py)Fe(II)(OH_2)]^{2+}$ (**1-OH$_2$**) to generate $[(N4Py)Fe(III)(OCH_3)]^{2+}$(**Error! Reference source not ound.**).

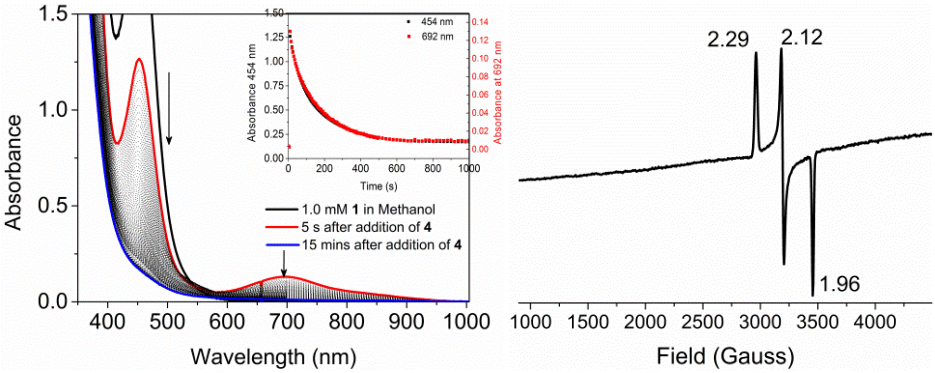


**Figure 89.** (left)UV-vis absorption spectrum changes of **1** (1 mM, 1 mL) in methanol before (black line) and 5 s after addition of 1 equiv **2** $[(N4Py)Fe(IV)=O]^{2+}$ (1 mM, 1 mL) (red line); final analytical concentrations of **1** and **2** are both 0.5 mM. Inset: Time dependence of the changes in absorbance at selected wavelengths. (right) X-band EPR spectrum of the flash frozen (at 77 K) sample taken after 15 minutes of reaction of **1** with 1 equiv **2** in methanol.

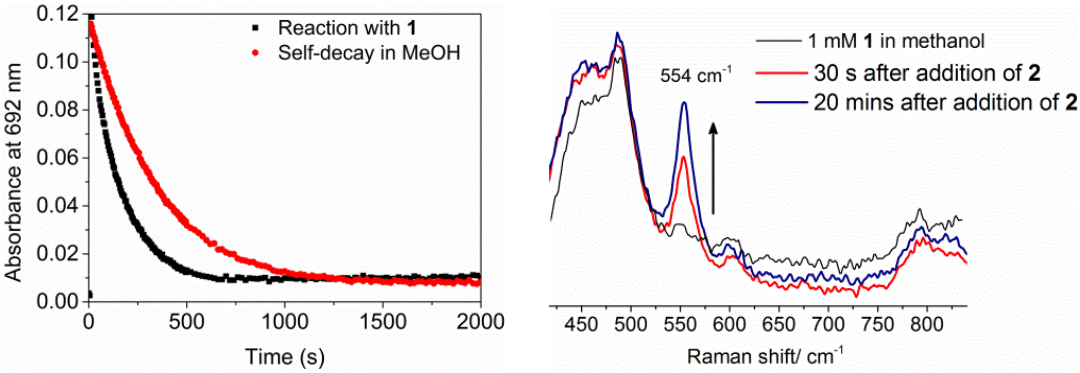


**Figure 90.** (left) Absorbance changes at 692 nm over time, (black) addition of 1 equiv **2** (1 mM, 1 mL) to **1** (1 mM, 1 mL) in methanol, (red) the self-decay of **2** in methanol (red). (right) Changes in Raman spectrum ($\lambda_{exc}$ 355 nm) of **1** (1 mM, 1 mL) in methanol (black), 30 s (red), and 20 minutes (blue) after addition of 1 equiv **2** (1 mM, 1 mL).

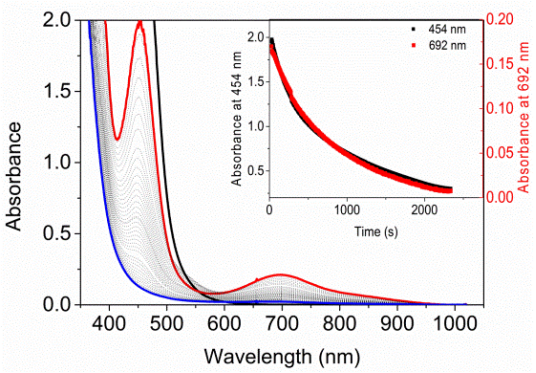


**Figure 91.** UV-vis absorption spectrum of **1** (1 mM, 1 mL) $CD_3OD$ before (black line), 1 s after addition of 1 equiv **2** $[(N4Py)Fe(IV)=O]^{2+}$ (1 mM, 1 mL) (red), following reaction (grey dotted-lines) and final spectrum is in blue, start analytical concentrations of **1** and **2** are both 0.5 mM. Inset: absorbance at 454 and 692 nm over time.

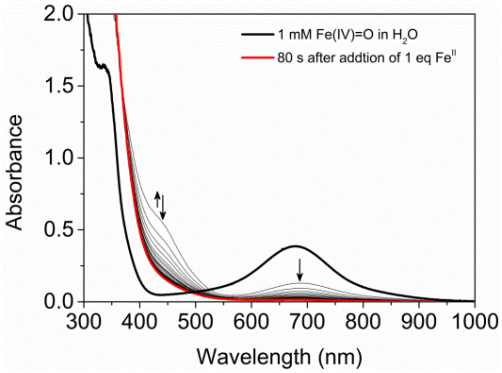


**Figure 92.** UV-vis absorption of **2** (1 mM, 1 mL) in $H_2O$, before (black), and after addition of 1 equiv **1-Cl** (1 mM, 1 mL in methanol) (grey lines) and final spectrum is in red, in which **1-Cl** was used due to the much higher solubility.

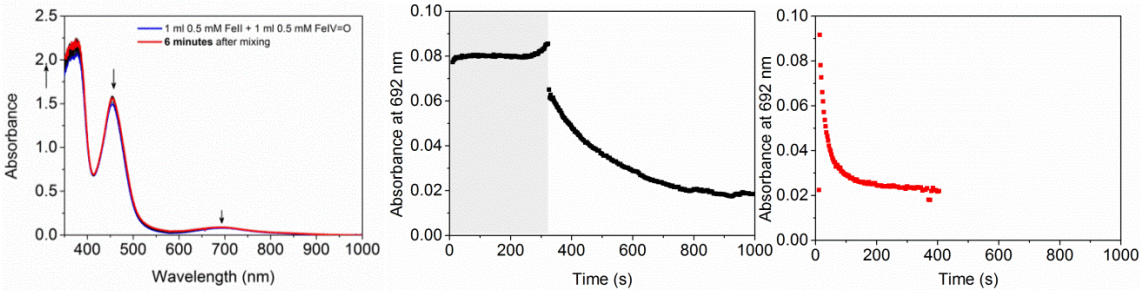


**Figure 93.** (Left) UV-vis absorption spectrum of **1** (0.25 mM) (blue), after addition of 1 equiv **2** (0.25 mM) in methanol at -30 °C (black lines), final spectrum is in red. (Middle) absorbance at 692 nm over time of the reaction of **1** (0.5 mM, 1 mL) with **2** (0.5 mM, 1 mL) in methanol at -30 °C: before (grey shadowed) and after (no shadow) addition of $H_2O$ (10 vol%). (Right) Absorbance at 692 nm over time of reaction of **1** (0.5 mM, 1 mL) with **2** in methanol at -30 °C (0.5 mM, 1 mL) in presence of $H_2O$ (50 vol%).

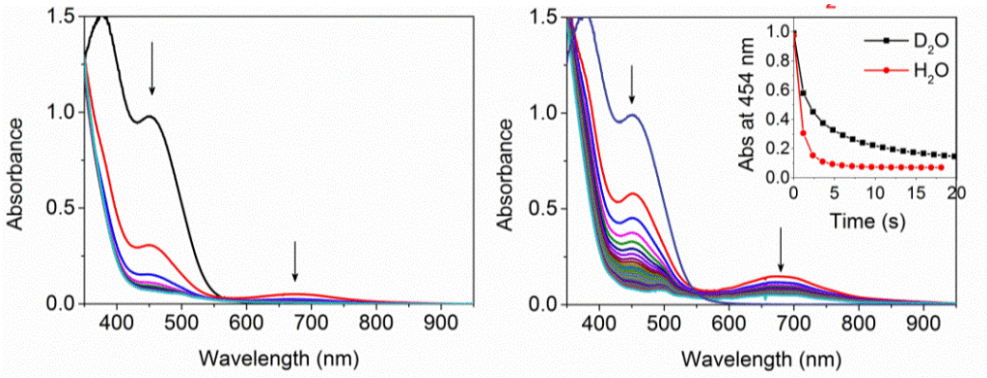


**Figure 94.** (Left) UV-vis absorption spectrum of **1** (0.5 mM, 1.2 mL) in $H_2O$ after addition of 1 equiv **2** (1.2 mM, 300 μL) in $H_2O$; (Right). UV-vis absorption spectrum of **1** (0.5 mM, 1.2 mL) in $D_2O$ after addition of 1 equiv **2** (1 2 mM, 300 μL) in $D_2O$.

Therefore, the 2:1 stoichiometry (**1**/$H_2O_2$) for the conversion of **1** to **4** (Fe(III)($OCH_3$)) in methanol is proposed in **Scheme 11**: upon dissolving, ligand exchange occurs immediately from **1** to form **1-OCH$_3$**, which engaged in a second ligand exchange with $H_2O_2$ (50 wt% in $H_2O$) to form Fe(II)OOH (**3**), followed by heterolysis to form **2** (Fe(IV)=O) (within the mixing time, < 1 s at 21 °C). **2** comproportionates with **1-OH$_2$** (formed by ligand exchange **1-OCH$_3$** with $H_2O$) to form **4** (Fe(III)-X, X = $OCH_3$, OH). Solvent deuteration retards comproportionation at certain extent, it allows the slightly accumulation of **2** (Fe(IV)=O), which results in the observation of minor amount of **2** by UV-vis spectroscopy (**Figure 83** and **Figure 84**). The reaction of $H_2O_2$ with **1** in methanol (spontaneous reaction) are much faster than with **2** (Fe(IV)=O) with $H_2O_2$ ($1.0 \times 10^{-2}$ $s^{-1}$ in $CH_3OH$, $1.0 \times 10^{-3}$ $s^{-1}$ in $CD_3OD$), so when **1-OCH$_3$** is present, there is no reaction between **2** and $H_2O_2$.

### 5.2.2 Reaction of 1 with near sub-stoichiometric $H_2O_2$ at -30 °C

Complex **1** shows temperature-dependent spin-crossover in both methanol (**Figure 95**) and $H_2O$ (**Figure 96**), which manifested in an increase in the molar absorptivity of the $^1$MLCT bands at 380 nm and 454 nm with decrease in temperature, and reversibly with increase in temperature (**Figure 96**).

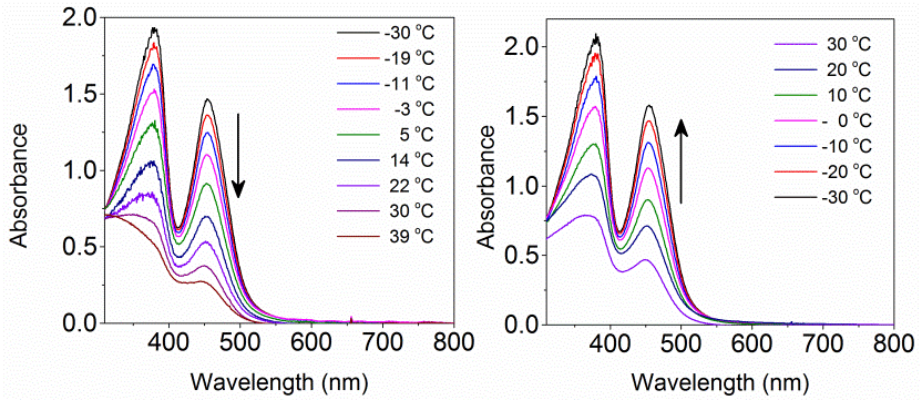


**Figure 95.** (Left) UV-vis absorption spectra changes of **1** (0.25 mM) in deoxygenated methanol with increase in temperature (-30 °C to 39 °C). (Right) UV-vis absorption spectra changes of **1** in methanol with decease in temperature (30 °C to -30 °C).

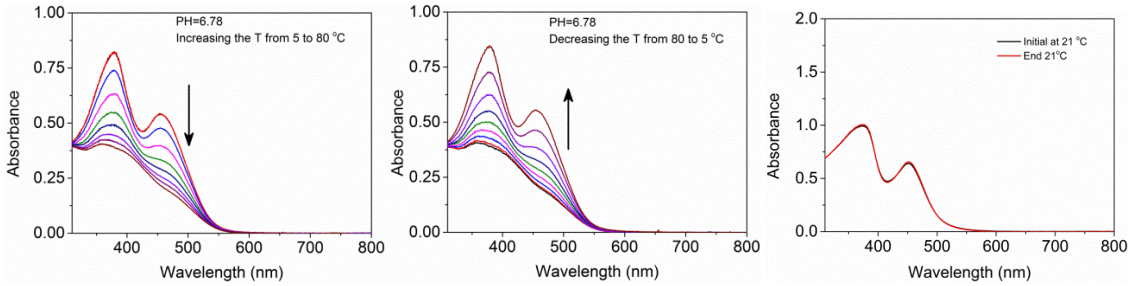


**Figure 96.** (Left) UV-vis absorption spectra changes of **1** (0.25 mM) in $H_2O$ with increase in temperature (-5 °C to 80 °C). (Middle) UV-vis absorption spectra changes of **1** in $H_2O$ with decease in temperature (80 °C to 5 °C). (Right) Comparison of UV-vis absorption spectrum of **1** in deoxygenated methanol (black) and the spectrum obtained by first increasing (21 °C to 40 °C) and then decreasing temperature (40 °C to -30 °C then to 21 °C).

As at 21 °C, step-wise addition of $H_2O_2$ to **1** in methanol at -30 °C results in the step-wise decrease of the absorbance at 454 nm, however, in contrast with that at 21 °C, the complete oxidation of **1** requires more than 0.5 equiv $H_2O_2$ (**Figure 97**). Furthermore, the NIR absorbance is unaffected, i.e. **2** (Fe(IV)=O) is not formed. Single-addition of 0.5 equiv $H_2O_2$ to **1** results in only 66% oxidation of **1**, but increases to 77% and > 90% in the presence of 5 and 10 vol% $H_2O$, respectively (**Figure 98** and **Figure 99**). This difference can be understood by consideration of the rates of each step in the multi-step reaction. At -30 °C (**Table 7**)，comproportionation between **2** (Fe(IV)=O) and **1** is much slower (**Figure 93**), and hence oxidation of **1** by comproportionation is not significant, so the oxidation of **1** by 0.5 equiv $H_2O_2$ is not feasible anymore. With addition of increasing amount of $H_2O$, the disproportionation pathway is also accelerated, which is consistent with full oxidation of **1** by 0.5 equiv $H_2O_2$ with presence of excess $H_2O$.

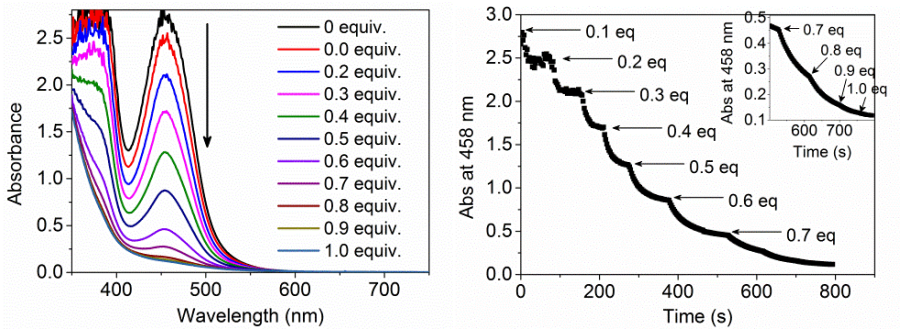


**Figure 97.** (left) UV-vis absorption spectra of stepwise addition of $H_2O_2$ to **1** (0.5 mM) in $CH_3OH$ at -30 °C. (right) Corresponding absorbance changes at 454 nm, inset is the expansion of region in 500 – 800 s.

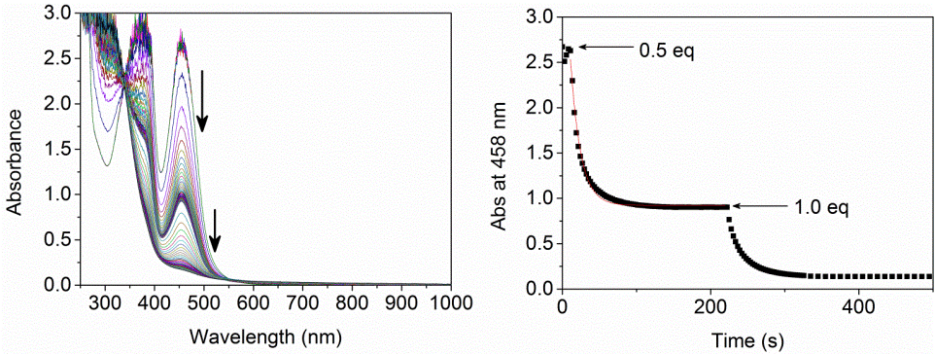


**Figure 98.** (left) UV-vis absorption spectrum changes of **1** in methanol at -30 °C with two-step addition of $H_2O_2$ (0.5 equiv for each step). (right) Corresponding absorbance changes at 454 nm.

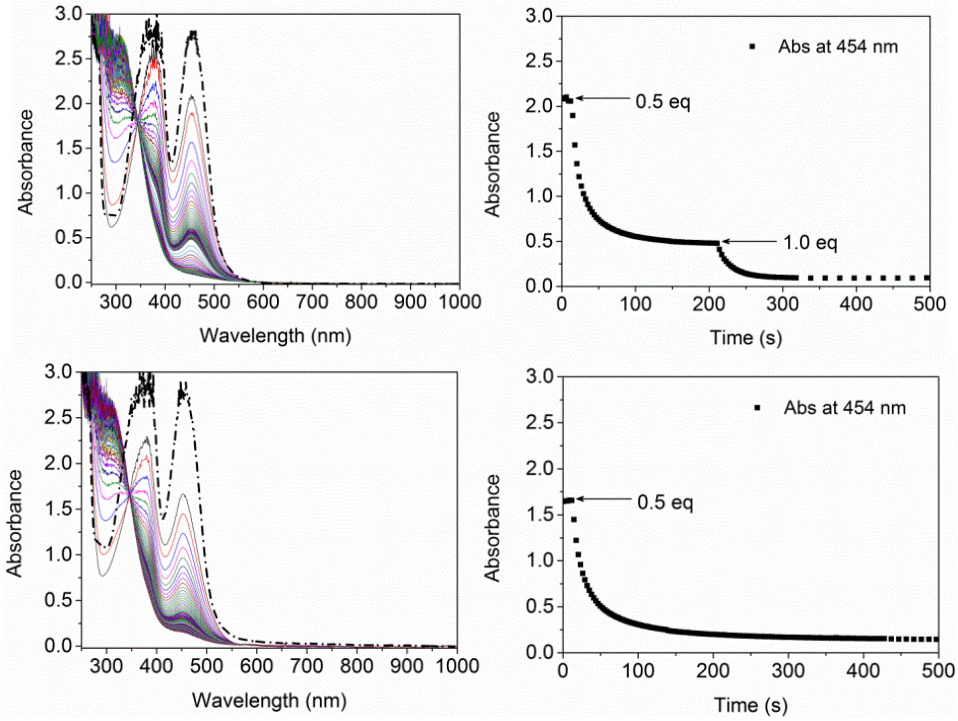


**Figure 99.** (left) UV-vis absorption spectrum changes of **1** in methanol with present of 5 vol% $H_2O$ (upper) and 10 vol% $H_2O$ (lower) at -30 °C with two-step addition of $H_2O_2$ (0.5 equiv for each step). (right) Corresponding absorbance changes at 454 nm.

### 5.2.3 Thermodynamic considerations

The calculated exergonicity (-18.5 kcal $mol^{-1}$) of O-O bond heterolysis in Fe(II)OOH (**3**) is consistent with absence of spectroscopic evidence for such an intermediate. The free energy changes for the proposed reactions (Scheme 11), indicates that dissolution of $^{1}$**1** in methanol is followed by ligand exchange of acetonitrile for methoxide as observed experimentally. The ligand exchange to form $[(N4Py)Fe^{II}(OOH)]^{+}$ ($^{5}$**3**) from $[(N4Py)Fe^{II}(OCH_3)]^{+}$ ($^{5}$**1-OCH$_3$**) is exergonic ligand (-3.7 kcal $mol^{-1}$), however, the subsequent O-O bond heterolysis to form $[(N4Py)Fe^{IV}O]^{+}$ ($^{3}$**2**) is highly exergonic (-18.5 kcal $mol^{-1}$). Adventitious water, together with water added with $H_2O_2$ (50 wt% in $H_2O$) can facilitate ligand exchange to form $[(N4Py)Fe(II)(OH_2)]^{2+}$ ($^{5}$**1-OH$_2$**) from $^{5}$**1-OCH$_3$** (-20.4 kcal $mol^{-1}$) also. As with earlier reports,[4] comproportionation between $^{5}$**1-OH$_2$** and $^{3}$**2** to form $[(N4Py)Fe(III)(OH)]^{2+}$ ($^{6}$**4-OH**) is highly exergonic (-13.3 kcal $mol^{-1}$) also. $[(N4Py)Fe(III)OMe]^{2+}$($^{6}$**4**), but not $^{6}$**4-OH** ($[(N4Py)Fe(III)(OH)]^{2+}$), were observed by Raman and EPR spectroscopy because of the exergonicity of the ligand exchange reaction with solvent (methanol).

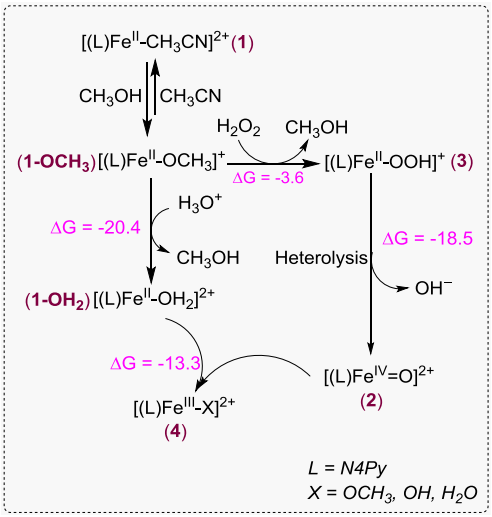


**Scheme 11.** Proposed reaction pathways for the formation $[(L)FeIII(OCH_3)]^{2+}$ with the calculated free energies (ΔG) for each step. Data include dispersion, entropic, and solvent corrections; unit is kcal/mol.

**Table 7.** Comparison of the observed rates of reactions

| | in methanol (rt) | in methanol (- 30 °C) | in $H_2O$ (rt) |
|---|---|---|---|
| $[(L)Fe^{IV}=O]$ Self-decay | $[(L)Fe^{IV}=O] \xrightarrow{k_{obs}}$ in $CH_3OH$: 1.0 mM, $1.8 \times 10^{-3}$ $s^{-1}$; 0.5 mM, $3.0 \times 10^{-3}$ $s^{-1}$; in $CD_3OD$: 0.5 mM, $6.48 \times 10^{-5}$ $s^{-1}$ | $[(L)Fe^{IV}=O]$ 0.5 mM $\xrightarrow[k_{obs}]{-30\ °C}$ in $CH_3OH$: no reaction; in $CD_3OD$: no reaction | $[(L)Fe^{IV}=O]$ 0.5 mM $\xrightarrow{k_{obs}}$ in $H_2O$: no reaction; in $D_2O$: no reaction |
| $[(L)Fe^{II}] + H_2O_2$ | $[(L)Fe^{II}\text{-}OCH_3] + H_2O_2$ (0.5 eq) $\xrightarrow{k_{obs}}$ in $CH_3OH$, fast, within mixing; in $CD_3OD$, fast, within mixing | $[(L)Fe^{II}\text{-}OCH_3]$ 0.5 mM + $H_2O_2$ (0.5 eq) $\xrightarrow[k_{obs}]{-30\ °C}$ in $CH_3OH$: $7.0 \times 10^{-2}$ $s^{-1}$; in $CD_3OD$: $5.0 \times 10^{-2}$ $s^{-1}$ | $[(L)Fe^{II}\text{-}OCH_3]$ 0.5 mM + $H_2O_2$ (0.5 eq) $\xrightarrow{k_{obs}}$ fast, within mixing |
| $[(L)Fe^{IV}=O] + H_2O_2$ | $[(L)Fe^{IV}=O]$ 1.0 mM + $H_2O_2$ (1 eq) $\xrightarrow{k_{obs}}$ $1.0 \times 10^{-2}$ $s^{-1}$; $[(L)Fe^{IV}=O]$ 1.0 mM + $D_2O_2$ (1 eq) $\xrightarrow{k_{obs}}$ $1.0 \times 10^{-3}$ $s^{-1}$ | $[(L)Fe^{IV}=O]$ 0.5 mM + $H_2O_2$ (0.5 eq) $\xrightarrow[k_{obs}]{-30\ °C}$ $3.0 \times 10^{-4}$ $s^{-1}$ | |
| $[(L)Fe^{IV}=O] + [(L)Fe^{II}]$ | $[(L)Fe^{IV}=O]$ 1.0 mM + $[(L)Fe^{II}\text{-}OCH_3]$ (1 eq) $\xrightarrow{k_{obs}}$ in $CH_3OH$, $6.0 \times 10^{-3}$ $s^{-1}$; in $CD_3OD$, $1.3 \times 10^{-3}$ $s^{-1}$ | $[(L)Fe^{IV}=O]$ 1.0 mM + $[(L)Fe^{II}\text{-}OCH_3]$ (1 eq) + $H_2O$: 0 vol%; 10 vol%; 50 vol%. $\xrightarrow[k_{obs}]{-30\ °C}$ $CH_3OH$: 0 vol%, no reaction; 10 vol%, $3.9 \times 10^{-3}$ $s^{-1}$; 50 vol%, $4.3 \times 10^{-2}$ $s^{-1}$ | $[(L)Fe^{IV}=O]$ 0.5 mM, + $[(L)Fe^{II}\text{-}OH_2]$ (1 eq) $\xrightarrow{k_{obs}}$ 1.12 $s^{-1}$; $[(L)Fe^{IV}=O]$ 0.5 mM + $[(L)Fe^{II}\text{-}OH_2]$ (1 eq) $\xrightarrow{k_{obs}}$ 0.4 $s^{-1}$ |

## 5.3 Conclusions

Earlier reports of the reactions of (TMC)$Fe^{II}$ and $Fe^{II}$(bispidine) complexes with $H_2O_2$, indicated strongly the direct formation of (L)$Fe^{IV}$=O via heterolysis of the O-O bond of (L)$Fe^{II}$-OOH intermediates. However, the observation of this reaction in these systems may reflect the lower potency of (TMC)$Fe^{IV}$=O in hydrogen-atom abstraction compared to that (N4Py)$Fe^{IV}$=O.[4,23] Hence, comproportionation of the ferrous and ferryl complexes is not significant in the former system. The homolytic cleavage mechanism in methanol proposed for the $Fe^{II}$(bispidine)/$H_2O_2$ systems is likely to be important, however, initial O-O bond heterolysis (Scheme 11) may be masked by subsequent comproportionation between $Fe^{II}$(bispidine) and FeIV=O, as well as the oxidation of $H_2O_2$ by $Fe^{IV}$=O, which were not considered earlier but shown for $Fe^{II}$(N4Py) in the present study. Both process rationalize the low yield formation (L)$Fe^{IV}$=O in $H_2O$ also.

## 5.4 Experimental section

**Synthesis.** The ligand 1,1-di(pyridin-2-yl)-N,N-bis(pyridin-2-ylmethyl)methanamine (N4Py), [(N4Py)Fe(II)($CH_3CN$)]($ClO_4$)$_2$ (**1**),[14] were prepared as reported previously. Commercially available chemicals were purchased from Sigma Aldrich without further purification. All solvents used for spectroscopy were of UVASOL (Merck) grade. Synthesis of ([(N4Py)Fe(IV)=O]($PF_6$)$_2$ (**4**).was available from previous study.[22].

### Computational details

Computational studies were performed using Gaussian 09, Revision D.01,15 as reported earlier.[19] Briefly, geometry optimization and frequency calculation were performed using an unrestricted hybrid density functional UB3LYP17–19 combined with CEP-31G20,21 basis set for iron and 6-311+g(d,p) for the rest of the atoms. Free energies (ΔG) on the energy profiles was obtained by UB3LYP-D3 energies and are corrected for zero point energy (ZPE), thermal and entropic corrections were made from frequency calculations at 298 K. The solvation energy was considered using water as a solvent with the SMD solvation model as implemented in Guassian09.

## 5.5 Acknowledgements

We thank Dr. Davide Angelone and Prof. Marcel Swart for the help with DFT calculations, Dr. Apparao Draksharapu Dr. Duenpen Unjaroen, Dr. Sandeep K. Padamati, and Dr. Ronald Hage for technical assistance and discussion, Prof. Carole Duboc for EPR studies and guidance in this projects. The Ministry of Education, Culture and Science of the Netherlands (Gravity program 024.001.035, W.R.B.), COST association action CM1305 ECOSTBio, the labex arcane (ANR-11-LABX-003), MINECO (CTQ2014-59212-P and CTQ2015-70851-ERC, M.S.), GenCat (2014SGR1202, M.S.), FEDER (UNGI10-4E-801, M.S.), FEDER (UNGI10-4E-801, M.S.), and the Chinese Scholarship Council (J.C.) are acknowledged for financial support.

## 5.6 References

(1) Costas, M.; Mehn, M. P.; Jensen, M. P.; Que, L. *Chem. Rev.* 2004, *104* (2), 939–986.
(2) Nam, W. *Acc. Chem. Res.* 2007, *40* (7), 522–531.
(3) Rohde, J.-U. *Science* 2003, *299* (5609), 1037–1039.
(4) Kaizer, J.; Klinker, E. J.; Oh, N. Y.; Rohde, J. U.; Song, W. J.; Stubna, A.; Kim, J.; Münck, E.; Nam, W.; Que, L. *J. Am. Chem. Soc.* 2004, *126* (2), 472–473.

(5) Kumar, D.; Hirao, H.; Que, L.; Shaik, S. *J. Am. Chem. Soc.* 2005, *127* (22), 8026–8027.
(6) Lim, M. H.; Rohde, J.-U.; Stubna, A.; Bukowski, M. R.; Costas, M.; Ho, R. Y. N.; Münck, E.; Nam, W.; Que, L. *Proc. Natl. Acad. Sci.* 2003, *100* (7), 3665–3670.
(7) Bukowski, M. R.; Koehntop, K. D.; Stubna, A.; Bominaar, E. L.; Halfen, J. A.; Münck, E.; Nam, W.; Que, L. *Science* 2005, *310* (5750), 1000–1002.
(8) Sastri, C. V; Sook Seo, M.; Joo Park, M.; Mook Kim, K.; Nam, W. *Chem. Commun.* 2005, *2* (11), 1405–1407.
(9) Costas, M.; Que, L. 2003, 3671–3673.
(10) Roelfes, G.; Lubben, M.; Hage, R.; Que, Lawrence, J.; Feringa, B. L. *Chem. – A Eur. J.* 2000, *6* (12), 2152–2159.
(11) Li, F.; England, J.; Que, L. *J. Am. Chem. Soc.* 2010, *132* (7), 2134–2135.
(12) Bautz, J.; Bukowski, M. R.; Kerscher, M.; Stubna, A.; Comba, P.; Lienke, A.; Münck, E.; Que, L. *Angew. Chemie Int. Ed.* 2006, *45* (34), 5681–5684.
(13) Draksharapu, A.; Li, Q.; Logtenberg, H.; van den Berg, T. A.; Meetsma, A.; Killeen, J. S.; Feringa, B. L.; Hage, R.; Roelfes, G.; Browne, W. R. *Inorg. Chem.* 2011, *51* (2), 900–913.
(14) Draksharapu, A.; Li, Q.; Logtenberg, H.; van den Berg, T. A.; Meetsma, A.; Killeen, J. S.; Feringa, B. L.; Hage, R.; Roelfes, G.; Browne, W. R. *Inorg. Chem.* 2011, *51* (2), 900–913.
(15) Bukowski, M. R.; Zhu, S.; Koehntop, K. D.; Brennessel, W. W.; Que, L. *J. Biol. Inorg. Chem.* 2004, *9* (1), 39–48.
(16) Tuschel, D. 2014, *29* (September), 1–7.
(17) Bukowski, M. R.; Comba, P.; Limberg, C.; Merz, M.; Que, L.; Wistuba, T. *Angew. Chemie Int. Ed.* 2004, *43* (10), 1283–1287.
(18) Liu, L. V; Hong, S.; Cho, J.; Nam, W.; Solomon, E. I. *J. Am. Chem. Soc.* 2013, *135* (8), 3286–3299.
(19) Draksharapu, A.; Angelone, D.; Quesne, M. G.; Padamati, S. K.; Gómez, L.; Hage, R.; Costas, M.; Browne, W. R.; de Visser, S. P. *Angew. Chemie Int. Ed.* 2015, *54* (14), 4357–4361.
(20) Oh, N. Y.; Suh, Y.; Park, M. J.; Seo, M. S.; Kim, J.; Nam, W. *Angew. Chemie* 2005, *117* (27), 4307–4311.
(21) Braymer, J. J.; O'Neill, K. P.; Rohde, J. U.; Lim, M. H. *Angew. Chemie - Int. Ed.* 2012, *51* (22), 5376–5380.
(22) Chen, J.; Draksharapu, A.; Harvey, E.; Rasheed, W.; Que, L.; Browne, W. R. *Chem. Commun.* 2017, *53* (91), 12357–12360.
(23) Sastri, C. V; Lee, J.; Oh, K.; Lee, Y. J.; Lee, J.; Jackson, T. A.; Ray, K.; Hirao, H.; Shin, W.; Halfen, J. A.; Kim, J.; Que, L.; Shaik, S.; Nam, W. *Proc. Natl. Acad. Sci.* 2007, *104* (49), 19181 LP-19186.